

# Defect line coarsening and refinement in active nematics

Nika Kralj,<sup>1</sup> Miha Ravnik,<sup>1,2</sup> and Žiga Kos<sup>1,2,3,\*</sup>

<sup>1</sup>*Faculty of Mathematics and Physics, University of Ljubljana, Jadranska 19, 1000 Ljubljana, Slovenia*

<sup>2</sup>*J. Stefan Institute, Jamova 39, 1000 Ljubljana, Slovenia*

<sup>3</sup>*Department of Mathematics, Massachusetts Institute of Technology,  
77 Massachusetts Avenue, Cambridge, MA 02139, USA*

(Dated: April 27, 2022)

Active matter naturally performs out-of-equilibrium which results in the emergence of diverse dynamic steady-states, including the omnipresent chaotic dynamic state known as active turbulence. However, much less is known how such active systems dynamically depart out of these configurations, such as get excited or damped to a different dynamic steady state. In this Letter, we demonstrate the transitional dynamics towards and between different dynamic steady states of three-dimensional active nematic turbulence, which we show is determined by the coarsening or refinement of the topological defect lines. Specifically, using theory and numerical modelling, we are able to predict the evolution of the active defect density away from the steady state as due to time-dependent activity or viscoelastic material properties, establishing a single length scale phenomenological description of defect line coarsening/refinement in a three-dimensional active nematic. The approach is first applied to growth dynamics of a single active defect loop, and then to a full three-dimensional active defect line network. The analysis also points out an interesting analogy with the coarsening dynamics of cosmic strings.

Active matter systems are distinctly non-equilibrium in nature, but regularly form dynamic steady states of diverse characteristics [1, 2]. Much like passive systems that evolve over time to reach equilibrium upon an external or internal stimulus, active systems can evolve into new or different dynamic steady states and the coarsening is observed as a major transitional mechanism [3–5]; for example a homogeneous suspension of self-propelled particles phase-separates and coarsens into dense and dilute regions [6, 7]. Density-density correlation functions during coarsening separate active suspensions into classes [8] with structure functions commonly deviating from the Porod’s law that is generally expected for systems relaxing towards equilibrium [8]. In active binary fluids, the initial length scale dynamics during coarsening is reported to follow the same time dependence as for passive fluids [9, 10], while at larger scales activity takes over and eventually a dynamical steady-state is established [9]. Coarsening was observed also in two-dimensional dry active nematics and is based on annihilation of half-integer defect pairs [11].

Active nematics are a class of active materials, which exhibit apolar orientational order along the director  $\mathbf{n}$ , with main material examples being microtubule mixtures and bacterial suspensions [2, 12–15]. In three dimensions, bulk active nematics form the dynamic steady state called active turbulence, which at the structural level is a dynamically rewiring network of defect lines and loops [16], driven by the anisotropic active stress [17]. At constant activity, active turbulence is in a dynamic equilibrium, where defect density fluctuates around a constant value, while the defects still move around and undergo structural reconfigurations [18, 19]. Defect line segments are driven by the self-propulsion velocity depending on their local director profile, leading the defect

loops to grow, shrink, and buckle in time [20, 21].

Beyond the active matter, the phase ordering kinetics through coarsening exhibits universal behaviour across a range of physical systems, as underlain with the fundamental role of the topological defects within the order parameter field [22]. Notably, the three-dimensional nematic systems have played a prominent role in demonstrating such universal behaviour for defects in the shape of lines and loops, since universal coarsening dynamics — first described by Kibble for cosmic strings [23] and later predicted by Zurek for superfluid helium [24] — was finally experimentally observed in nematic liquid crystals [25]. Universal rules for phase kinetics are typically obtained through energetic arguments [22], which opens a question what novel insights active matter energetics as an emergent field can provide.

In this Letter, we show transitional dynamics towards and between dynamic steady states of 3D active nematic turbulence, as distinctly determined by the coarsening and refinement of a network of topological defect lines and loops. We construct an analytical model of the collapse or growth of a single defect loop and then generalise it to the coarsening/refinement of the full 3D defect network. The approach provides analytic insight into the effective phase ordering kinetics towards dynamic steady states, as triggered by changes in the main material parameters, such as activity or even nematic elasticity and viscosity. While the notion of self-propelled defects is unique for active nematics, the demonstrated coarsening-refinement indicates possible universal behaviour applicable to different physical systems, including cosmic string dynamics.

Active nematics are described by the experimentally supported [16, 26] mesoscopic active nematodynamic formulation [27, 28]. The approach is based on the coupled

dynamics of two main fields — the velocity field  $\mathbf{v}$  and the nematic order parameter tensor  $\mathbf{Q}$  with the director  $\mathbf{n}$  as the main eigenvector. Flow field is determined by the active propulsion due to the active stress that is proportional to  $\mathbf{Q}$  [17], and by the viscous coupling to the nematic order, whereas the dynamics of  $\mathbf{Q}$  is determined by the interplay between the dissipative relaxation towards the equilibrium and coupling to the material flow. Specifically, we solve this model by using a hybrid lattice Boltzmann algorithm with the results given in units of mesh resolution  $\Delta x$ , tensorial elastic constant  $L$ , and rotational viscosity  $\Gamma$  (for more on modelling and parameters see Supplemental Material (SM)). Indeed, such numerical approach was shown to reproduce different structural and dynamical features of multiple experimental two-dimensional [29, 30] and three-dimensional active nematic systems [16, 19, 20].

Coarsening of a defect network of three-dimensional active turbulence is demonstrated in Fig. 1, following a quench from a high defect density regime numerically generated by a random director field initial condition. This coarsening dynamics shows gradually decreasing defect density, but notably also includes both shrinking *and* expansion of the topological defects (see dynamic changes in Fig. 1). The kinetics of isolated active defect loops can be captured as the competition between the (elastic) line tension and the active propulsion, subjected to the viscous drag of the moving defect. We calculate these competing mechanisms for an inplane zero-topological charge loop of radius  $r$  as shown in Fig. 2a (i.e.  $+1/2$  winding number on the left and  $-1/2$  on the right). The line tension — which originates from the effective elastic nature of nematic materials — can be estimated as  $T = \frac{\pi K}{4} \ln \frac{r}{r_{\min}}$ , where  $K$  is the single elastic constant, and  $r_{\min}$  is the lower radial bound of the region associated with the defect line [31]. The viscous drag force on the defect line originates from local rotations of the director field as the defect core moves through the material and can be written as  $\Gamma v = \frac{\pi}{4} \gamma_1 v \ln \frac{r}{r_{\min}}$ , where  $\gamma_1$  is the rotational viscosity and  $v$  the velocity of the defect line segment. And the active propulsion can be estimated by using self-propulsion velocities  $v_0$  for different defect loop segments [20, 32]; for the  $+1/2$  defect loop section, we take  $v_0 \approx \frac{|\alpha|r}{4\eta}$ , where  $\alpha$  is the activity and  $\eta$  the effective isotropic viscosity, whereas for the  $-1/2$  section we assume no self-propulsion. Finally, assuming a radial loop (compare to full numerical calculations in Fig. 2a), all these contributions give a dynamical equation for the active nematic defect loop radius

$$\dot{r} = \frac{v_0}{2} - \frac{T}{\Gamma r} = \frac{|\alpha|r}{8\eta} - \frac{K}{\gamma_1 r}. \quad (1)$$

Solving the Eq. 1 gives the time dependence of loop ra-

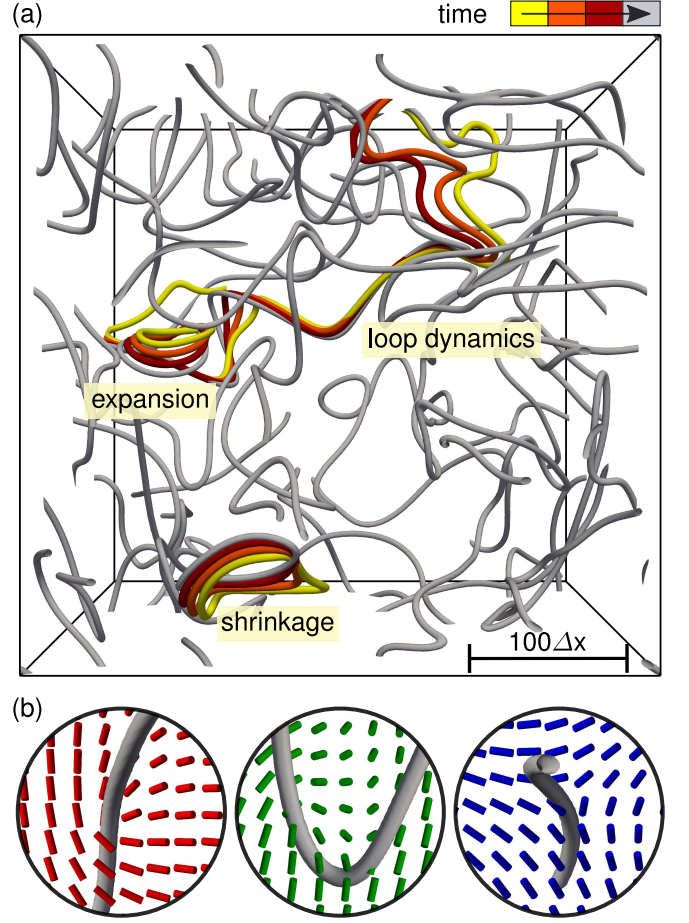


FIG. 1. **Coarsening dynamics of the active nematic turbulence.** (a) A snapshot of a defect line network during coarsening process. All topological defects at selected time are shown in gray, and selected defect line segments are drawn in different colours at selected earlier time intervals  $50 \Delta x^2 / (\Gamma L)$  apart. (b) The director field rotates for an angle of  $\pi$  around the defect lines: from  $+1/2$  profiles (red), to twist (green) and  $-1/2$  profiles (blue).

dus

$$r(t) = r_c \left[ 1 + \left( \frac{r_0^2}{r_c^2} - 1 \right) e^{t/\tau_{\text{loop}}} \right]^{1/2}, \quad (2)$$

where characteristic time scale of isolated defect loops  $\tau_{\text{loop}} = \frac{4\eta}{|\alpha|}$ ,  $r_0$  is the initial loop radius at  $t = 0$ , and

$r_c = \sqrt{\frac{8\eta K}{\gamma_1 |\alpha|}}$  is the critical radius for which the active-propulsion exactly counterbalances the loop line tension (i.e.  $\dot{r} = 0$ ). Note, how  $r_c$  is explicitly dependent on nematic elasticity, activity and rotational viscosity, which provides a direct analytic insight into possible control of active defect loop kinetics; namely, for  $r > r_c$  the loops expand, whereas for  $r < r_c$  the loops shrink.

The analytical model is compared to the full numerical simulation, observing excellent agreement as shown in Fig. 2. A loop with a fixed initial radius is let to dynam-

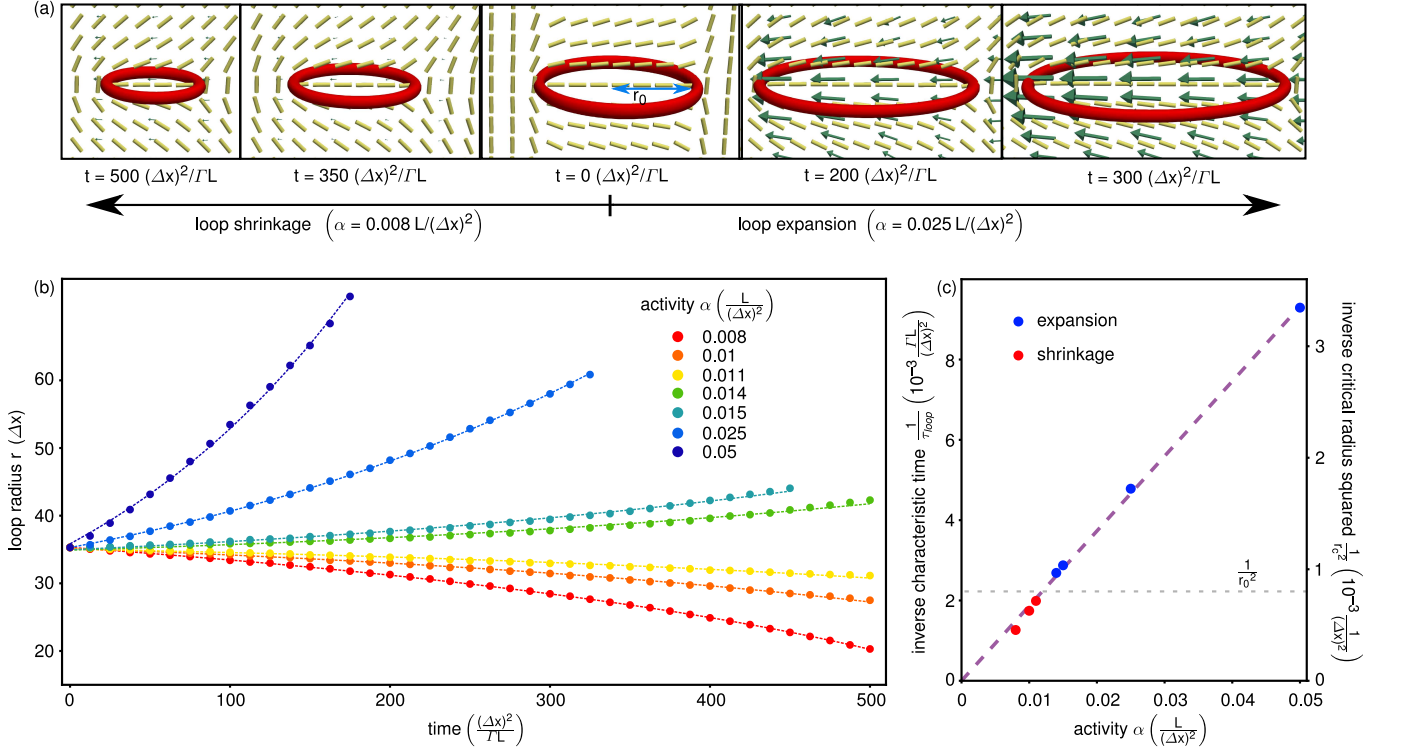


FIG. 2. **Shrinking and expanding dynamics of isolated active nematic defect loop.** (a) Depending on activity  $\alpha$ , the defect loop either shrinks or expands in time; the panels show defect loop as isosurface of degree of order (red), director field (yellow rods), and velocity field (green arrows). The defect loop has  $+1/2$  winding number (2D topological charge) at the left side, and  $-1/2$  winding number on the right side, which generates an overall self propulsion velocity and a local active stress on the loop towards the left. (b) Single loop radius as function of time for different activities. Radius is determined as the loop left-to-right dimension in panel (a). Dashed line is a fit (Eq. 2) to the numerical data with fit parameters  $\tau_{\text{loop}}$  and activity-independent parameter  $r_c^2/\tau_{\text{loop}}$ , obtaining  $r_c^2/\tau_{\text{loop}} = 2.78 \Gamma L$ . (c) Shrinking and expanding dynamics as determined by the activity-dependent critical radius and initial radius  $r_0 = 35.3 \Delta x$  (dashed line). A linear dependence of  $1/\tau_{\text{loop}}$  (or equally  $1/r_c^2$ ) on activity is obtained with the slope of  $1/\tau_{\text{loop}} = 0.186 \Gamma \alpha$ .

ically evolve at different activities and depending on the activity, this leads to shrinking (Supplementary Movie 1) or expanding (Supplementary Movie 2) dynamics. A fit of Eq. 2 to the simulation data gives  $1/\tau_{\text{loop}} = 0.186 \Gamma \alpha$  and  $r_c^2/\tau_{\text{loop}} = 2.78 \Gamma L$ , which compares well to values of  $1/\tau_{\text{loop}} = 0.182 \Gamma \alpha$  and  $r_c^2/\tau_{\text{loop}} = 2 \Gamma L$  that are calculated directly from the viscoelastic parameters of the simulation. More generally, now supported also by the numerical simulations, we show that the nematic elasticity, active propulsion and the viscous drag are the main mechanisms that affect the overall kinetics of the three-dimensional active defects.

The mechanisms of defect line tension, drag force and self propulsion that were used to describe the single active defects can be generalised to the overall coarsening dynamics of a full three-dimensional defect network of the active turbulence. We use a single scale model based on a single time-dependent length scale  $\xi$ , which represents both typical radius of curvature and typical separation of defect lines [25, 31]. Notice that during active coarsening, we observe that both the average defect-defect separation and the curvature decrease over time, as shown in

Fig. 3(a,b). Specifically,  $\xi$  is calculated as  $\rho = 1/\xi^2$  where  $\rho$  is the total defect length over unit volume. The coarsening dynamics of the defect networks is now described as the time evolution of the single length-scale  $\xi$  based on a balance between the defect line tension  $T/\xi$  and viscous drag  $\Gamma(\dot{\xi} + b v_0)$ , where the dimensionless phenomenological parameter  $b$  describes the effective self-propulsion velocity of defect line of any half-integer director profile. Generalized from a single defect loop (Eq. 1) to a defect network, here the line tension straightens and spaces out the defects in time, which gives the main dynamic equation of active coarsening

$$\dot{\xi} = a \frac{K}{\gamma_1 \xi} - b \frac{|\alpha| \xi}{4\eta}, \quad (3)$$

where in analogy to the passive coarsening [33, 34], we use dimensionless parameter  $a$  to describe the relative strength of line tension compared to drag force in a defect network. Equation 3 can be rewritten in terms of the

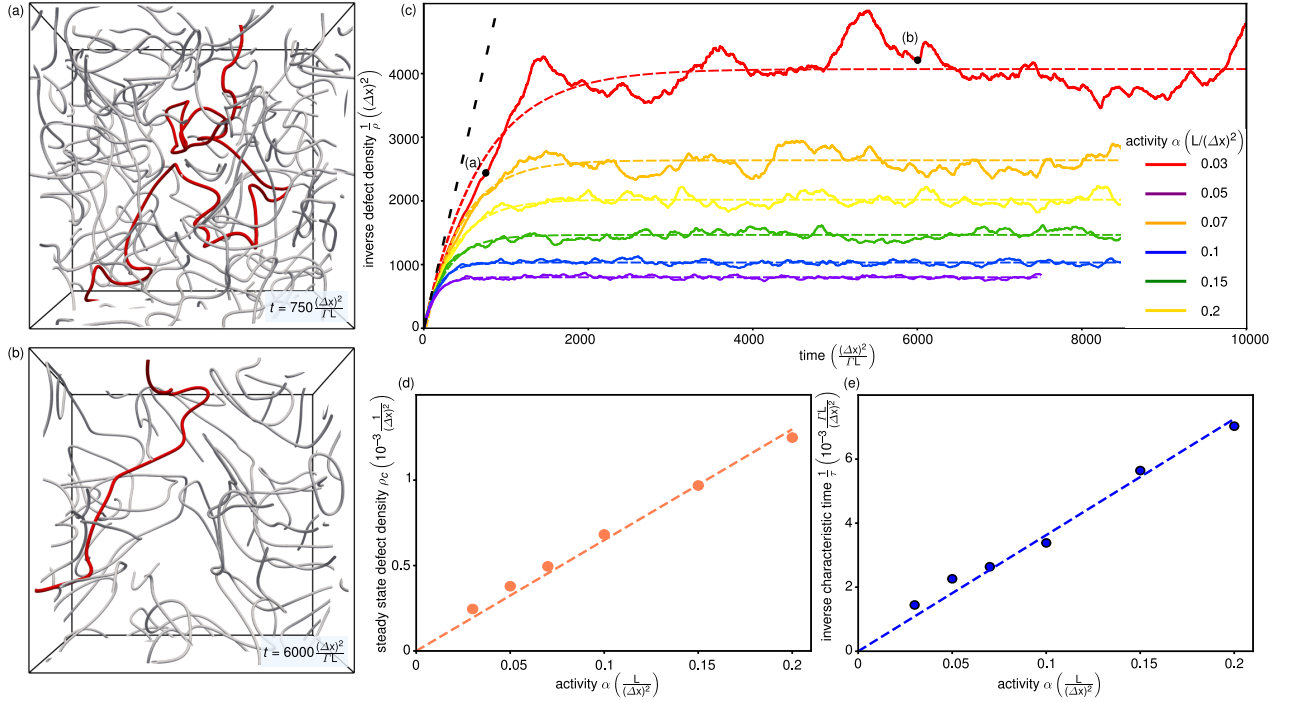


FIG. 3. **Coarsening dynamics of 3D active nematic turbulence.** (a) Defect network at short time in the coarsening dynamics. A selected connected defect segment is colored in red. (b) Defect network at later time in the coarsening dynamics. Defect line segments are further apart and show smaller curvature compared to (a). (c) Inverse defect density over time for different activities. Dashed lines are fits of Eq. 5 to the simulation data. Black dashed line represents the activity-independent initial density dynamics. The fluctuations of the defect density at later times is the effect of the finite simulation volume but with a well determined average. (d) Steady-state defect density as dependent on activity; linear fit (dashed line) has the slope of  $0.0065/L$ . (e) Linear dependence of the inverse characteristic time on activity; the linear fit has coefficient of  $0.036\Gamma$ . Points in (d) and (e) are obtained from fits in (c).

defect density as

$$\dot{\rho} = \frac{b|\alpha|}{2\eta}\rho - \frac{2aK}{\gamma_1}\rho^2, \quad (4)$$

and upon integration at constant activity, the coarsening equation for the active defect density is obtained as

$$\rho(t) = \rho_c \left[ 1 + \left( \frac{\rho_0}{\rho_c} - 1 \right) e^{-t/\tau} \right]^{-1}, \quad (5)$$

where the characteristic coarsening time of the active turbulence is  $\tau = \frac{2\eta}{b|\alpha|}$ ,  $\rho_c = \frac{b|\alpha|\gamma_1}{4\eta aK}$  is the steady-state defect density and  $\rho_0$  is the initial density at  $t = 0$ . We should emphasise that Eq. 4 can describe a more general dynamic evolution of the topological defect density (i.e. going beyond constant parameters in Eq. 5), as caused by any immediate or gradual dynamic change in the broad set of material parameters including activity, elasticity, and viscosity that can be additionally dependent on externally-imposed fields, such as temperature or pressure.

Numerical modelling of active coarsening dynamics of 3D active turbulence — using full active nematodynamics based on  $\mathbf{Q}$  and velocity field  $\mathbf{v}$  (see SM) — is shown

in Fig. 3 and Supplementary Movie 3. The simulations are performed from an initial configuration of a random director field at each data point and in  $\sim 400$  time steps ( $t \approx 10 \Delta x^2/(\Gamma L)$ ) a dense defect network is formed, which coarsens over time (Fig. 3c, Fig. S1). For high defect density at short times after quench, we observe that the coarsening dynamics is independent on activity (Fig. 3c), which can be explained by the elastic tension being much larger than the active self-propulsion; note the linear vs. quadratic dependent terms on  $\rho$  in Eq. 4. At later times, the defect density approaches the steady-state density  $\rho_c$ , which we find is linearly proportional to activity (Fig. 3d), in full agreement with the analytical model ( $\rho_c$  in Eq. 5). The rate of approach towards  $\rho_c$  is governed by the time scale  $\tau$ , which is inversely proportional to activity (Fig. 3e). Dimensionless parameters  $a$  and  $b$  from the analytical model can now be determined by a linear fit in Figs. 3(d,e), obtaining  $a = 2.8$  and  $b = 0.10$ . Parameter  $a$  is of roughly similar magnitude as in passive (i.e. zero activity) nematics [33], whereas a low value of the phenomenological parameter  $b$  indicates that the defects on average are repelled from each other with a much lower velocity than  $v_0$ , which is characteristic for a  $+1/2$  profile and was included in the director



cross-section for a single loop dynamics in Fig. 2.

Active refinement is — oppositely to coarsening — characterized by the proliferation of defects (for example induced by an increase of activity) and we show that it is governed by the same main mechanisms of defect line tension and active propulsion. The notable difference between coarsening and refinement is that for refinement the activity prevails over the line tension. Figure 4 and Supplementary Movie 4 show the defect density upon active refinement. The observed refinement dynamics from full numerical simulations is compared to the coarsening-refinement model introduced in Eq. 4 and a good agreement is found. Figure 4 also shows that the rate of the activity change affects the refinement dynamics, as it has to be compared to the characteristic coarsening/refinement time  $\tau(t)$ . Fast changes in activity (red line in Fig. 4) can still be described by constant activity dynamics (Eq. 5), whereas for other regimes (blue and green lines in Fig. 4) the full time-dependent activity  $\alpha(t)$  has to be considered in Eq. 4. More generally, the results show that the introduced approach also well covers the *time-dependent* changes in the active nematic material parameters, including not only time-dependent activity, but also elasticity, viscosity and other, indicating an exciting analytic insight into the kinetics of active states out of the dynamic equilibrium.

Experimentally, the demonstrated active coarsening (or refinement) could be induced by possible (meso)phase transitions into or from a nematic phase due to a pressure or a temperature quench, as achievable in passive liquid crystals [25, 35]. It could potentially be induced also by changes of activity as the nematic material parameters that control the isotropic-nematic phase transition are known to be activity-dependent [36], and activity is known to be capable of inducing phase transitions in self-propelled particles [37]. By using different change rates of pressure, temperature, or activity, active nematic phase transition could be studied also in view of early-stage domain growth as described by a Kibble-Zurek mechanism, which is known to describe structure formation in liquid crystals [38, 39], and could interestingly be additionally coupled to curved interfaces [40] and topology of the confining space [41].

The demonstrated coarsening and refinement of active defects shows also interesting implications beyond soft and active matter. Distinctly, at zero activity, the coarsening dynamics of nematic defect strings is known to share strong mathematical similarities with cosmic strings and condensed matter systems [23, 24], whereas here we show that activity can contribute new coarsening terms. Namely, in an active nematic system, the time derivative of the characteristic length scale  $\xi$  (Eq. 3) equals an elastic term proportional to  $1/\xi$  and an active term proportional to  $\xi$ . This active coarsening dynamics has interesting analogies with the velocity-dependent one-scale cosmic string model [42, 43], where (i) the fric-

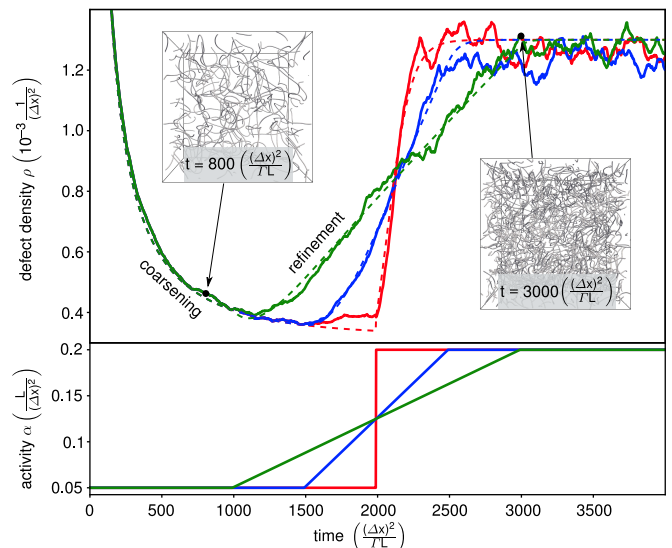


**FIG. 4. Active refinement induced by time-varying activity.** Defect density (top graph) is shown for the three different time-varying activities (bottom graph). Note the matching colors. The dynamics is initiated (at  $t = 0$ ) from a random director field initial condition, leading first to coarsening which upon an activity increase changes to refinement. Dashed lines are fits with Eq. 4.

tion term due to particle scattering proportional to  $1/\xi$  is known to give the Kibble coarsening scaling  $\xi \sim t^{0.5}$ , and (ii) the term proportional to  $H\xi$ , where  $H$  is the Hubble parameter, accounts for the expansion of the universe. Both terms in the cosmic string model are positive and promote the coarsening dynamics, whereas for active nematics the  $\xi$  term is negative ( $\dot{\xi} \sim -\xi$ ) and as we demonstrate can slow down the coarsening and leads to a dynamic steady-state with a finite defect density. Such a term would correspond to coarsening of a string network in a shrinking universe. More generally, this analogy provides novel unprecedented parallels between active matter and cosmology.

The authors acknowledge funding from Slovenian Research Agency (ARRS) under contracts P1-0099, N1-0124, J1-1697, J1-2462, N1-0195, and from European Research Council grant LOGOS.

\* ziga.kos@fmf.uni-lj.si

- [1] G. Gompper, R. G. Winkler, T. Speck, A. Solon, C. Nardin, F. Peruani, H. Löwen, R. Golestanian, U. B. Kaupp, L. Alvarez, T. Kiørboe, E. Lauga, W. C. K. Poon, A. DeSimone, S. Muñoz-Landin, A. Fischer, N. A. Söker, F. Cichos, R. Kapral, P. Gaspard, M. Ripoll, F. Sagues, A. Doostmohammadi, J. M. Yeomans, I. S. Aranson, C. Bechinger, H. Stark, C. K. Hemelrijk, F. J. Nedelec, T. Sarkar, T. Aryaksama, M. Lacroix, G. Duclos,

- V. Yashunsky, P. Silberzan, M. Arroyo, and S. Kale, The 2020 motile active matter roadmap, *J. Phys.: Condens. Matter* **32**, 193001 (2020).
- [2] M. C. Marchetti, J. F. Joanny, S. Ramaswamy, T. B. Liverpool, J. Prost, M. Rao, and R. A. Simha, Hydrodynamics of soft active matter, *Rev. Mod. Phys.* **85**, 1143 (2013).
  - [3] D. Geyer, D. Martin, J. Tailleur, and D. Bartolo, Freezing a Flock: Motility-Induced Phase Separation in Polar Active Liquids, *Phys. Rev. X* **9**, 031043 (2019).
  - [4] G. S. Redner, M. F. Hagan, and A. Baskaran, Structure and Dynamics of a Phase-Separating Active Colloidal Fluid, *Phys. Rev. Lett.* **110**, 055701 (2013).
  - [5] F. Fadda, D. A. Matoz-Fernandez, R. van Roij, and S. Jabbari-Farouji, Dynamical steady-states of active colloids interacting via chemical fields, *arXiv:2203.05213 [cond-mat.soft]* (2022).
  - [6] S. Chakraborty and S. K. Das, Relaxation in a phase-separating two-dimensional active matter system with alignment interaction, *J. Chem. Phys.* **153**, 044905 (2020).
  - [7] G. Gonnella, D. Marenduzzo, A. Suma, and A. Tiribocchi, Motility-induced phase separation and coarsening in active matter, *Comptes Rendus Physique* **16**, 316 (2015).
  - [8] S. Dey, D. Das, and R. Rajesh, Spatial Structures and Giant Number Fluctuations in Models of Active Matter, *Phys. Rev. Lett.* **108**, 238001 (2012).
  - [9] S. Berti, G. Boffetta, M. Cencini, and A. Vulpiani, Turbulence and Coarsening in Active and Passive Binary Mixtures, *Phys. Rev. Lett.* **95**, 1 (2005).
  - [10] S. Sabrina, M. Spellings, S. C. Glotzer, and K. J. M. Bishop, Coarsening dynamics of binary liquids with active rotation, *Soft Matter* **11**, 8409 (2015).
  - [11] S. Mishra, S. Puri, and S. Ramaswamy, Aspects of the density field in an active nematic, *Phil. Trans. R. Soc. A* **372**, 20130364 (2014).
  - [12] T. Sanchez, D. T. N. Chen, S. J. DeCamp, M. Heymann, and Z. Dogic, Spontaneous motion in hierarchically assembled active matter, *Nature* **491**, 431 (2012).
  - [13] H. H. Wensink, J. Dunkel, S. Heidenreich, K. Drescher, R. E. Goldstein, H. Lowen, and J. M. Yeomans, Mesoscale turbulence in living fluids, *Proc. Natl. Acad. Sci.* **109**, 14308 (2012).
  - [14] R. Alert, J. Casademunt, and J.-F. Joanny, Active Turbulence, *Annu. Rev. Condens. Matter Phys.* **13** (2022).
  - [15] J. Hardoüin, J. Laurent, T. Lopez-Leon, J. Ignés-Mullol, and F. Sagués, Active microfluidic transport in two-dimensional handlebodies, *Soft Matter* **16**, 9230 (2020).
  - [16] G. Duclos, R. Adkins, D. Banerjee, M. S. E. Peterson, M. Varghese, I. Kolvin, A. Baskaran, R. A. Pelcovits, T. R. Powers, A. Baskaran, F. Toschi, M. F. Hagan, S. J. Streichan, V. Vitelli, D. A. Beller, and Z. Dogic, Topological structure and dynamics of three-dimensional active nematics, *Science* **367**, 1120 (2020).
  - [17] Y. Hatwalne, S. Ramaswamy, M. Rao, and R. Simha, Rheology of Active-Particle Suspensions, *Phys. Rev. Lett.* **92**, 118101 (2004).
  - [18] J. Urzay, A. Doostmohammadi, and J. M. Yeomans, Multi-scale statistics of turbulence motorized by active matter, *J. Fluid Mech.* **822**, 762 (2017).
  - [19] Ž. Krajnik, Ž. Kos, and M. Ravnik, Spectral energy analysis of bulk three-dimensional active nematic turbulence, *Soft Matter* **16**, 9059 (2020).
  - [20] J. Binysh, Ž. Kos, S. Čopar, M. Ravnik, and G. P. Alexander, Three-dimensional Active Defect Loops, *Phys. Rev. Lett.* **124**, 257 (2020).
  - [21] C. Long, X. Tang, R. L. B. Selinger, and J. V. Selinger, Geometry and mechanics of disclination lines in 3d nematic liquid crystals, *Soft Matter* **17**, 2265 (2021).
  - [22] A. J. Bray, Theory of phase-ordering kinetics, *Adv. Phys.* **51**, 481 (2010).
  - [23] T. W. B. Kibble, Topology of cosmic domains and strings, *J. Phys. A: Math. Gen.* **9**, 1387 (1976).
  - [24] W. Zurek, Cosmological experiments in condensed matter systems, *Phys. Rep.* **276**, 177 (1996).
  - [25] I. Chuang, R. Durrer, N. Turok, and B. Yurke, Cosmology in the laboratory: Defect dynamics in liquid crystals, *Science* **251**, 1336 (1991).
  - [26] F. G. Woodhouse and R. E. Goldstein, Spontaneous Circulation of Confined Active Suspensions, *Phys. Rev. Lett.* **109**, 168105 (2012).
  - [27] S. Čopar, J. Aplinc, Ž. Kos, S. Žumer, and M. Ravnik, Topology of Three-Dimensional Active Nematic Turbulence Confined to Droplets, *Phys. Rev. X* **9**, 031051 (2019).
  - [28] L. N. Carenza, G. Gonnella, D. Marenduzzo, and G. Negro, Rotation and propulsion in 3d active chiral droplets, *Proc. Natl. Acad. Sci.* **116**, 22065 (2019).
  - [29] A. Doostmohammadi, J. Ignés-Mullol, J. M. Yeomans, and F. Sagués, Active nematics, *Nat. Commun.* **9**, 045006 (2018).
  - [30] R. Zhang, Y. Zhou, M. Rahimi, and J. J. de Pablo, Dynamic structure of active nematic shells, *Nat. Commun.* **7**, 13483 (2016).
  - [31] M. Kleman and O. Lavrentovich, *Soft Matter Physics: An Introduction* (Springer, New York, 2003).
  - [32] L. Gioni, M. J. Bowick, P. Mishra, R. Sknepnek, and M. C. Marchetti, Defect dynamics in active nematics, *Phil. Trans. R. Soc. A* **372**, 20130365 (2014).
  - [33] B. Yurke, A. Pargellis, T. Kovacs, and D. Huse, Coarsening dynamics of the XY model, *Phys. Rev. E* **47**, 1525 (1993).
  - [34] W. Wang, T. Shiwaku, and T. Hashimoto, Experimental study of dynamics of topological defects in nematic polymer liquid crystals, *J. Chem. Phys.* **108**, 1618 (1998).
  - [35] D. Austin, E. J. Copeland, and T. W. B. Kibble, Evolution of cosmic string configurations, *Phys. Rev. D* **48**, 5594 (1993).
  - [36] S. P. Thampi, A. Doostmohammadi, R. Golestanian, and J. M. Yeomans, Intrinsic free energy in active nematics, *EPL* **112**, 28004 (2015).
  - [37] M. E. Cates and J. Tailleur, Motility-induced Phase Separation, *Annu. Rev. Condens. Matter Phys.* **6**, 219 (2015).
  - [38] Z. Bradač, S. Kralj, and S. Žumer, Early stage domain coarsening of the isotropic-nematic phase transition, *J. Chem. Phys.* **135**, 024506 (2011).
  - [39] N. Fowler and D. I. Dierking, Kibble-Zurek Scaling during Defect Formation in a Nematic Liquid Crystal, *ChemPhysChem* **18**, 812 (2017).
  - [40] N. Stoop and J. Dunkel, Defect formation dynamics in curved elastic surface crystals, *Soft Matter* **14**, 2329 (2018).
  - [41] M. Nikkhou, M. Škarabot, S. Čopar, M. Ravnik, S. Žumer, and I. Mušević, Light-controlled topological charge in a nematic liquid crystal, *Nature Phys.* **11**, 183 (2015).
  - [42] C. J. A. P. Martins and E. P. S. Shellard, Extending

the velocity-dependent one-scale string evolution model, Phys. Rev. D **65**, 575 (2002).  
 [43] C. Martins, I. Rybak, A. Avgoustidis, and E. Shel-

---

lard, Stretching and Kibble scaling regimes for Hubble-damped defect networks, Phys. Rev. D **94**, 1 (2016).

## APPENDIX

### Details on numerical modeling

We perform extensive mesoscale simulations of active nematics based on the Beris-Edwards approach to nematodynamics extended with the active stress tensor [17, 27–30]. The approach is based on a set of coupled dynamic equations for the orientational order (given by the Q-tensor) and the fluid velocity  $\mathbf{v}$ . The Q-tensor evolves as

$$(\partial_t + v_k \partial_k) Q_{ij} - S_{ij} = \Gamma H_{ij}, \quad (6)$$

where  $\mathbf{v}$  is the fluid velocity and  $\Gamma$  is the rotational viscosity coefficient. The generalized advection term  $S_{ij}$  includes the effects of velocity gradients on the nematic order

$$S_{ij} = (\chi D_{ik} - \Omega_{ik}) \left( Q_{kj} + \frac{1}{3} \delta_{kj} \right) + \left( Q_{ik} + \frac{1}{3} \delta_{ik} \right) (\chi D_{kj} + \Omega_{kj}) - 2\chi \left( Q_{ij} + \frac{1}{3} \delta_{ij} \right) Q_{kl} W_{lk}, \quad (7)$$

where  $\chi$  is the flow alignment parameter,  $D_{ij} = \frac{1}{2}(\partial_i v_j + \partial_j v_i)$  and  $\Omega_{ij} = \frac{1}{2}(\partial_i v_j - \partial_j v_i)$  are symmetric and antisymmetric part of the velocity gradient tensor  $W_{ij} = \partial_i v_j$ , respectively, and  $H_{ij} = -\delta F / Q_{ij} + \frac{1}{3} \delta_{ij} \text{Tr}(\delta F / \delta Q_{ij})$  is the molecular field that drives system towards the equilibrium of the free energy  $F$ . The free energy is written in the Landau-de Gennes single elastic form as

$$F = \int \left( \frac{A}{2} Q_{ij} Q_{ji} + \frac{B}{3} Q_{ij} Q_{jk} Q_{ki} + \frac{C}{4} (Q_{ij} Q_{ji})^2 + \frac{L}{2} (\partial_k Q_{ij})^2 \right) dV, \quad (8)$$

where  $A$ ,  $B$  and  $C$  are material parameters and  $L$  is the elastic constant. The flow field obeys the continuity equation  $\partial_t \rho + \partial_i (\rho v_i) = 0$  and the Navier-Stokes equation  $\rho (\partial_t + v_j \partial_j) v_i = \partial_j \Pi_{ij}$ , where  $\rho$  is the fluid density and  $\Pi_{ij}$  is the stress tensor, consisting a passive and an active term  $\Pi_{ij} = \Pi_{ij}^{\text{passive}} + \Pi_{ij}^{\text{active}}$ ,

$$\begin{aligned} \Pi_{ij}^{\text{passive}} = & -p \delta_{ij} + 2\chi \left( Q_{ij} + \frac{1}{3} \delta_{ij} \right) Q_{kl} H_{kl} - \chi H_{ik} \left( Q_{kj} + \frac{1}{3} \delta_{kj} \right) - \chi \left( Q_{ik} + \frac{1}{3} \delta_{ik} \right) H_{kj} + \\ & + Q_{ik} H_{kj} - H_{ik} Q_{kj} + 2\eta D_{ij} - \partial_i Q_{kl} \frac{\delta F}{\delta \partial_j Q_{kl}}, \end{aligned} \quad (9)$$

$$\Pi_{ij}^{\text{active}} = -\alpha Q_{ij}, \quad (10)$$

where  $p$  is the pressure,  $\eta$  is the isotropic viscosity and  $\alpha$  is the activity, which is positive in extensile materials and negative in contractile materials. The coupled equations for the nematic order and the fluid velocity are solved numerically using the hybrid lattice-Boltzmann approach [27, 28, 30]. This approach consists of finite difference method for solving the Q-tensor evolution (Eq. 6), and the D3Q19 lattice Boltzmann method for the Navier-Stokes equation and the continuity equation.

The simulations of loop shrinkage and expansion were performed on a  $300 \times 300 \times 300$  mesh size, while the coarsening dynamics were obtained on a  $400 \times 400 \times 400$  mesh. Periodic boundary conditions were used in all the directions of the simulation box. Mesh resolution is defined as  $\Delta x = 1.5\xi_n$ , where  $\xi_n$  is nematic correlation length  $\xi_n = \sqrt{L/(A + BS_{eq} + \frac{9}{2}CS_{eq}^2)}$  and  $S_{eq}$  is the equilibrium value of the scalar order parameter. The results of the simulations are expressed in the units of the mesh resolution  $\Delta x$ , rotational viscosity parameter  $\Gamma$  and elastic constant  $L$ . The time step in case of loop dynamics is set to  $\Delta t = 0.0025 (\Delta x)^2 / (\Gamma L)$ . In the coarsening and refinement dynamics the time step equals  $\Delta t = 0.025 (\Delta x)^2 / (\Gamma L)$ . The following values of the model parameters are used:  $A = -0.43L/(\Delta x)^2$ ,  $B = -5.3L/(\Delta x)^2$ ,  $C = 4.325L/(\Delta x)^2$ ,  $S_{eq} = 0.533$ ,  $\eta = 1.38/\Gamma$ , and  $\chi = 1$ . Elasticity  $L$  and viscosity  $\Gamma$  parameters in the Q-tensor formulation of nematodynamics can be expressed with the parameters  $K$  and  $\gamma_1$  from the director formulation as used in Eq. 1 using the relations:  $\gamma_1 = 9S^2/(2\Gamma)$  and  $K = 9LS^2/2$ , where  $S$  is the scalar order parameter.



## Supplementary Figures

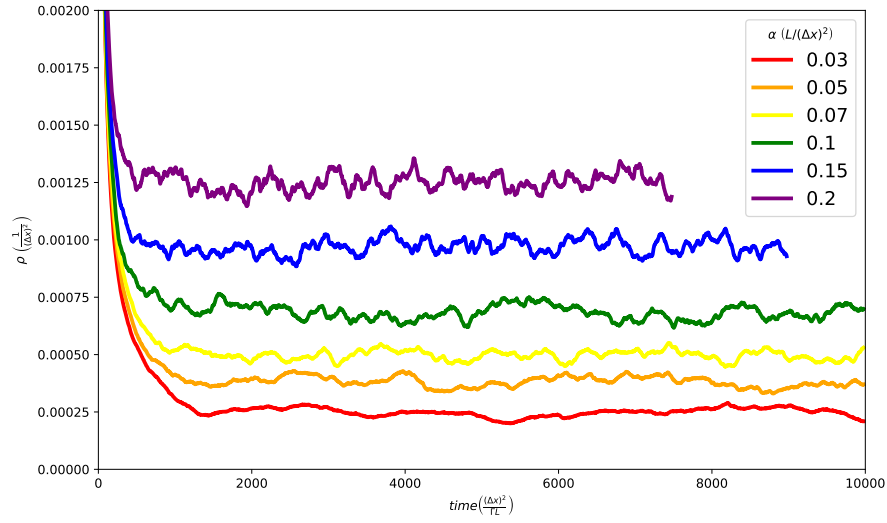


FIG. S1. Coarsening dynamics of three-dimensional active nematic defect networks. Defect density is shown over time for different activities. The numerical simulation is started from random director field initial condition. The coarsening leads to activity-dependent dynamic steady states, described by the steady state defect density  $\rho_c$ . The defect density is defined as the length of defect lines over a unit volume and is computed from the defect volume fraction that describes defect regions where scalar order parameter is  $S < 0.4$ .

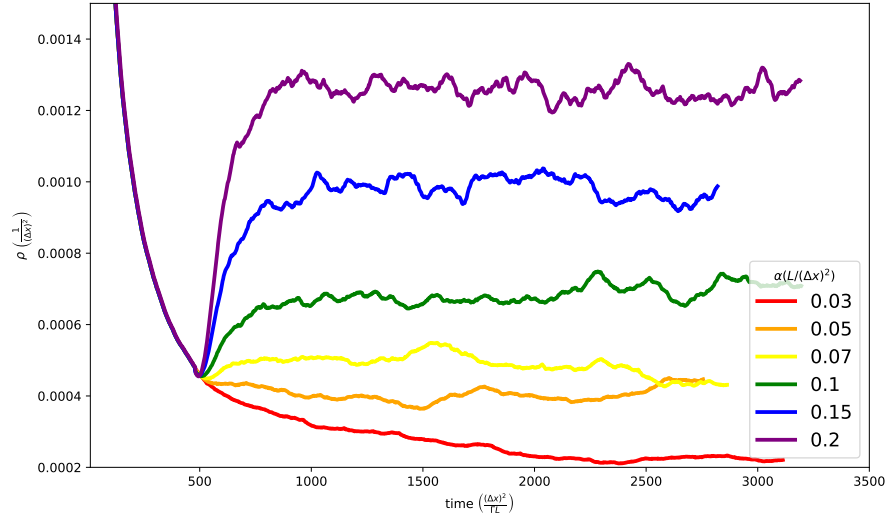


FIG. S2. Active coarsening and refinement for three-dimensional active nematics. The coarsening dynamics is started from a random director field initial condition at zero activity. At  $t = 500 (\Delta x)^2 / (\Gamma L)$ , the activity is increased to a finite value. If the activity is increased to a small value, the coarsening dynamics is slowed down. At higher activity increase, the coarsening dynamics turns to refinement and the defect density is increased.